Energy spectra of collisionally produced H^- autodetaching states*

J. S. Risley,† A. K. Edwards,‡ and R. Geballe
Department of Physics, University of Washington, Seattle, Washington 98195
(Received 8 October 1973)

Several lines, observed between 9 and 30 eV in the energy spectra of electrons ejected in 100-eV to 10-keV collisions of H^- with He, Ar, and H_2, are attributed to autodetaching states of H^-. The energy of the lowest line associated with the $(2s^2)\,^1S$ state of H^- was found to be 9.59 ± 0.03 eV. Two lines due to Ar^- autodetaching states were used to calibrate the energy scale. The separations in energy between the $(2s^2)\,^1S$ line of H^- and several other lines lying below the $n=2$ and $n=3$ levels of hydrogen were measured. The present results agree well with theoretical predictions and with the experimentally observed resonances in the elastic scattering of electrons on atomic hydrogen.

I. INTRODUCTION

Electron loss is the most important inelastic process in negative-ion collisions. The energy spectrum of the detached electrons can consist of lines corresponding to autodetaching excited states of the negative ion superimposed on a background continuum of directly detached electrons. In ion-atom collisions one can learn about the nature of the doubly excited states by making precise spectral measurements of the ejected electrons.

During the past decade many spectral observations have been made of the electrons produced in positive-ion–atom and atom-atom collisions.[1] In the case of negative-ion–atom collisions only a few systems have been studied. In 1967 Bydin[2] observed a line in I^- collisions with rare-gas targets which can be attributed to an autodetaching state of I^-. Several lines collisionally produced by O^- were observed in 1971 by Edwards, Risley, and Geballe[3] and in 1973 by Edwards and Cunningham,[4] and lines from Cl^- were reported also in 1973 by Cunningham and Edwards.[5] In this paper, we report on the electron energy spectra arising from keV collisions of H^- with He, Ar, and H_2.

Until recently,[6] autodetaching states of H^- were observed only as resonances (or compound states) in the elastic scattering cross section for electrons on atomic hydrogen[7-13] and as resonances in the Lyman-α production cross section by electron impact.[14,15] Normally the observed e-H resonance consists of a highly asymmetric peak owing to interference with the background cross section. In order to extract the position and width of the resonance in elastic scattering from an experimental observation the character of the potential (or nonresonant) scattering cross section has to be well known theoretically. Also, if a line is narrow, an $e^- + H$ experiment might miss or average over the resonance if the energy spread of the incident electron or hydrogen beam is larger than the resonance. On the other hand, in an experiment using heavy-body collisions, the strength of a line in the electron spectrum corresponding to an autodetaching state depends only on the production or excitation cross section and not on the decay width of the state if the width is sufficiently narrow. Also, in heavy-body collisions, there are few selection rules governing the excitation of differing angular momentum states.

The two-electron H^- system is one of the simplest physical systems to describe quantum mechanically. However, since H^- is a three-body system, exact energy levels and wave functions cannot be found. H^- has received, therefore, much attention as a proving ground for the validity of approximations prior to their extension to more-complicated systems.

Several excellent reviews have been written which deal with resonances in e-H scattering; see Burke,[16] Smith,[17] Chen,[18] and Schulz.[19]

Although no bound excited levels have been observed or calculated below the detachment limit ($\frac{3}{4}$ eV) of H^-,[20-22] doubly excited states in which both electrons are promoted into outer orbitals have been calculated theoretically and observed experimentally (see below). These levels lie above the detachment limit of H^- and both electron and photon deexcitation can occur. Because the coupling between the excited H^- and the continuum state consisting of an H atom plus free electron is usually quite strong, the transition probability for electron emission from these states is large, 10^{14} sec^{-1}, compared with the transition probability for optical radiation, 10^7 to 10^9 sec^{-1}. One expects,

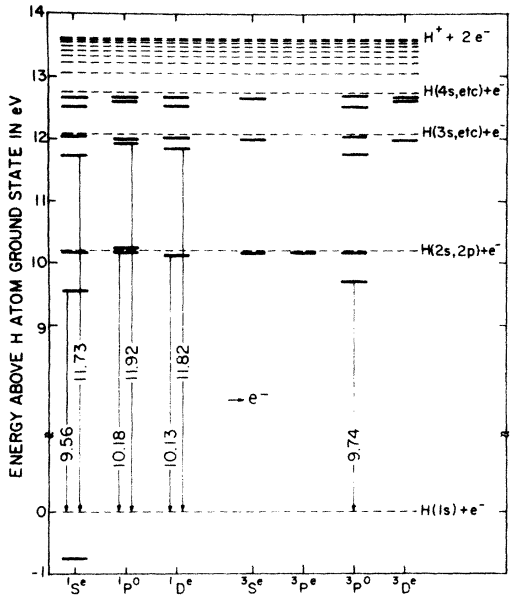

FIG. 1. Energy-level diagram of H^- showing the autodetaching transitions observed in this experiment.

therefore, that if the transition is allowed, the excited state of H^- will decay almost exclusively via electron emission.

It should be noted that the independent electron-configuration assignment $(nln'l')$ is not necessarily a good basis set for describing H^-. Eigenstates are more properly described by quantum numbers corresponding to an electron in the field of a dipole. The total spin and total angular momentum of the state are, however, good quantum numbers. Since reasonably accurate wave functions for the lower-lying states of H^- can be made from series expansions consisting predominately of single independent electron configurations, it has become customary to use the atomic-orbital description in identifying H^- states.

Figure 1 shows an energy-level diagram for H^- based on theoretical calculations listed in the Appendix. Also included are the transitions observed in this experiment.

In the present experiment, H^- was excited in a single collision with a neutral target particle:

$$H^-(1s^2)\,{}^1S + A \rightarrow H^{-*}(nln'l') + A,$$

$$H^{-*}(nln'l') \rightarrow H(1s) + e^-,$$

where n and $n' \geq 2$. The energy distribution of the ejected electrons exhibited several lines superimposed on a continuum. On the other hand, the continuum electrons were produced primarily by direct, single-electron detachment from H^-. With He as a target particle, two lines were observed below the $n=2$ level (10.2 eV) of H. Two additional lines appeared using H_2 as a target gas, one below the $n=2$ level and one below $n=3$. Using Ar, two additional lines corresponding to autodetaching states of Ar^- were observed and used to calibrate the energy scale.

The lines observed in the ejected electron spectra at higher collision energies in this experiment are believed to originate in transitions from states of a free negative hydrogen ion since most decays occurred well outside of the interaction region. The interaction or excitation time for keV H^- collisions is on the order of 10^{-16} sec. The lifetime of the autodetaching states is greater than 10^{-14} sec. The position and width of the lines were, however, strongly influenced by kinematic effects.

II. EXPERIMENTAL PROCEDURE

A. Apparatus

Since this apparatus has been described elsewhere,[3,23,24] only a brief summary will be given here. Figure 2 shows the general layout of the

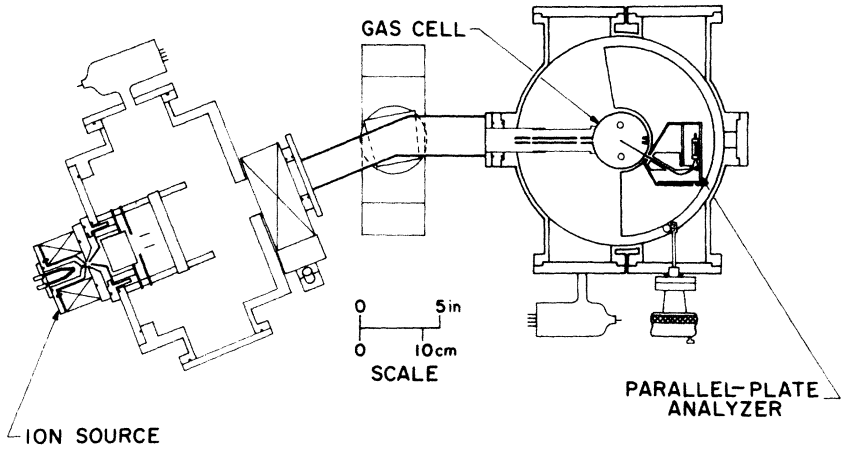

FIG. 2. General layout of the apparatus.

apparatus. H^- ions were extracted from a duoplasmatron ion source,[25] focused into a beam and magnetically mass analyzed. The kinetic energy of the ions could be varied between 75 eV and 10 keV. The current was typically 10^{-7} A. The ion beam passed into a cylindrical cell containing the target gas. The pressure of the gas, typically $(5-10)\times10^{-4}$ Torr, was measured using a Baratron capacitance manometer. A narrow slot was cut through the cylindrical gas cell, which allowed electrons to pass into an electron spectrometer. An electrostatic electron energy analyzer was mounted on a rotatable platform outside the gas cell to allow measurements to be made continuously at angles from 9° to 80° with respect to the ion-beam direction. The platform was geared to a rotary feedthrough located outside the vacuum chamber. The electrons were counted individually using a continuous electron multiplier. Pulses from the electron multiplier were amplified and counted either with a scaler or a countrate meter. The electron energy distribution was recorded using an X-Y recorder for dominant features, a signal averager for small signals, or single-channel analysis (point by point) for precise measurement of the peaks. In the last case, a Gaussian line profile was fitted numerically to the data to determine the center and full width at half-maximum (FWHM) of the line. The analyzer deflection voltage was measured to within 1 mV using a differential voltmeter which was calibrated against National Bureau of Standards voltage sources. The region surrounding the gas cell in which the analyzer was situated could be differentially pumped to less than 10^{-5} Torr when the cell was filled to 5×10^{-4} Torr. Magnetic fields due to the earth's field and the ion-beam mass-analyzing magnet were annulled to less than 20 mG using three pairs of mutually perpendicular, 61-cm-diam Helmholtz coils. Electric fields inside the gas cell and analyzer owing to contact potential and surface charges were reduced by painting all surfaces with Aquadag and depositing gold black on top of the Aquadag.[26] This treatment also reduced the electron reflectivity of the surfaces. Two second-order focusing electron analyzers were used in this study: a high-resolution cylindrical-mirror analyzer and a 30° parallel-plate deflection analyzer.

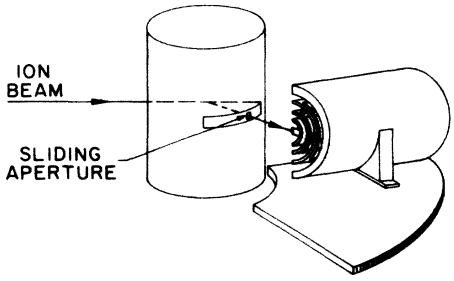

FIG. 3. Cylindrical mirror analyzer and gas cell.

The second-order focusing cylindrical-mirror analyzer used in this experiment has been described in more detail in a recent article by Risley.[24] Figure 3 shows the arrangement of the gas cell and the cylindrical-mirror analyzer. A sliding aperture (slit) which served as the first collimating aperture was attached to the side of the cylindrical gas cell. Both the slit and analyzer could be rotated as a unit. The beam of electrons passed through the coaxis of the cylinders at an angle of 42.5°. The resolution of the cylindrical-mirror analyzer was measured using a beam of 30-eV electrons from a cathode-ray tube assembly. Figure 4 shows the FWHM of the line versus the electron energy. The resolution (0.45%) was determined from the slope of a straight line which was fitted to the experimental data. The diameters of the entrance slit and exit slit were 0.4 and 0.2 mm, respectively. The dispersion was 7.2 cm. The calculated resolution was 0.43%. The analyzer constant C, defined as the proportionality constant between the analyzer deflection voltage V_d and the kinetic energy E of the electron,

$$V_d = CE,$$

was 1.002 ± 0.005.[23,24]

Some measurements were also made with a second-order focusing parallel-plate analyzer. The electrons entered this analyzer at 30°—the proper angle for second-order focusing.[27] The fringing fields were reduced by using electrodes inserted between the outer edges of the front and back electrodes and set at appropriate potentials to maintain a constant electric field inside the analyzer. The entrance and exit slits were ad-

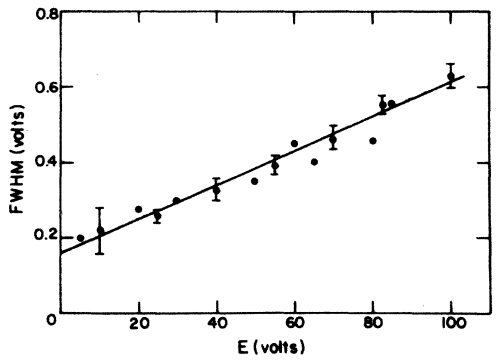

FIG. 4. FWHM versus electron energy for the cylindrical mirror analyzer. The resolution determined from the slope of the straight line was 0.45%.

justable so that the energy resolution and solid angle subtended by the detector could be set at any desired value. A Spiraltron electron multiplier (Bendix Corp.), placed behind the exit slit, detected the electrons. The analyzer was placed inside a tight box so that stray electrons would not be detected. With the width of the entrance and exit slits set at 0.2 mm each, the resolution was 1%. The dispersion was 3 cm. The calibration constant C was 0.999 ± 0.001.[23]

All spectral measurements were made with constant analyzing energy for which a constant voltage V_{an} was applied between the front and back electrodes of the analyzer.[23,28,29] All electrons, then, were analyzed at the same energy and the same resolution. Using this mode the energy separations between line spectra were measured to a high accuracy that depended only on the precision of the deflection voltage V_d:

$$eV_d = E + [(C-1)/C]\,eV_{an}, \tag{1}$$

where E is the kinetic energy of the electron. With C equal to unity, the analyzer reads the energy directly. If V_{an} is constant for two different electron energies E_1 and E_2,

$$eV_{d_1} - eV_{d_2} = E_1 - E_2. \tag{2}$$

Care was taken to ensure that no electric field between the gas cell and front electrode penetrated the constant electric field inside the analyzer. Any penetration would invalidate Eq. (2) since V_{an} would not be independent of the voltage V_d.

B. Reaction kinematics

In this experiment, the electrons emitted from the excited H^- ions were kinematically shifted in energy owing to the ion velocity. This effect has been described before by Rudd *et al.*,[30] Gordeev and Ogurtsov,[31] and Gerber, Morgenstern, and Niehaus.[32] However, the previous treatments do not contain sufficient detail to cover the large kinematic effects we encountered in the present experiment with keV H^- ions. A somewhat more general discussion is presented here.

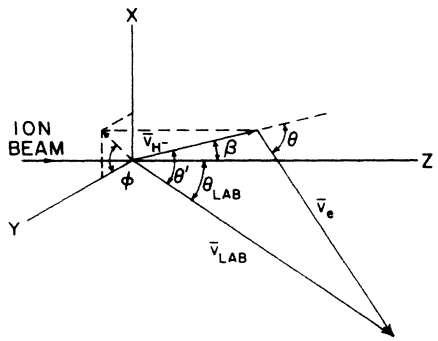

FIG. 5. Velocity vector diagram showing kinematic effect of ion velocity on the ejected electron. $\bar{v}_{H^-}$ is the H^--ion velocity scattered into a cone of angle β. $\bar{v}_{lab}$, in the y-z plane, is the observed velocity of the ejected electron.

Figure 5 is a velocity vector diagram showing the addition of the velocity $\bar{v}_{H^-}$ of the ion to the velocity $\bar{v}_e$ of the ejected electron. The ion velocity $\bar{v}_{H^-}$ is about 10 eV less than the initial velocity of the ion beam because of the energy loss in the excitation of H^-. The equation relating the velocities is

$$\bar{v}_e = \bar{v}_{lab} - \bar{v}_{H^-}, \qquad v^2_e = v^2_{lab} + v^2_{H^-} - 2v_{lab}\,v_{H^-}\cos\theta', \tag{3}$$

where

$$\cos\theta' = \cos\theta_{lab}\cos\beta + \sin\theta_{lab}\sin\beta\cos\phi,$$

$\bar{v}_{lab}$ is the velocity of the electron in the laboratory frame, and θ_{lab} is the observation angle defined with respect to the ion-beam axis. The angle at which the ion is deflected away from the ion axis by the collision is defined by the cone angle β, and ϕ is the azimuthal angle between $\bar{v}_{lab}$ and $\bar{v}_{H^-}$. For this experiment the H^--ion velocity was always less than that of the ejected electron. It is assumed that there was no correlation between the azimuthal angle ϕ and the observation angle θ_{lab}.

Equation (3) does not agree exactly with the expression for the kinematic shift given in a paper by Gordeev and Ogurtsov.[31] They made the unstated approximation that $(m/M_{ion})E_{ion} \ll E$, and thus their equation and ensuing discussion is somewhat restricted.

The equation relating the unshifted energy E of the ejected electron to the H^--ion energy E_{H^-} and laboratory energy E_{lab} is

$$E = E_{lab} + (m/M)E_{H^-} - 2[(m/M)\,E_{lab}\,E_{H^-}]^{1/2}\cos\theta', \tag{4}$$

where $m/M = 1/1838$ is the ratio of the mass of the electron to the mass of the H^- ion. Since our experiment did not distinguish between differing azimuthal angles between the scattered ion and ejected electron, an average over ϕ was taken for the shifted energy of the electrons using the expression

$$\langle E_{lab}\rangle_{av} = (2\pi)^{-1}\int_0^{2\pi} E_{lab}\,d\phi, \tag{5}$$

where

$$E_{lab} = E + (m/M)\,E_{H^-}(2\cos^2\theta' - 1) + 2\cos\theta'\{(m/M)E_{H^-}[E + (m/M)E_{H^-} \times(\cos^2\theta' - 1)]\}^{1/2}.$$

The shifted laboratory energy of the electrons is given by the approximate expression

$$\langle E_{\rm lab}\rangle_{\rm av} \simeq E + (m/M)E_{\rm H^-}(2\cos^2\theta_{\rm lab}\cos^2\beta - 1) + 2\cos\theta_{\rm lab}\cos\beta\{(m/M)E_{\rm H^-}[E + (m/M)E_{\rm H^-} \times(\cos^2\theta_{\rm lab}\cos^2\beta - 1)]\}^{1/2}. \quad (6)$$

For convenience, the bars are dropped and $E_{\rm lab}$ will be used for $\langle E_{\rm lab}\rangle_{\rm av}$ in the remainder of this paper. It was found that for the precision of this experiment β was sufficiently small so that $\cos\beta$ could be set equal to unity.[23]

For the ion energies used in this experiment, the laboratory energy of the 9.6-eV H^- ^1S line could be shifted to values ranging from $\frac{1}{2}$ to 30 eV depending on ion energy and observation angle. Figure 6 shows the laboratory energy $E_{\rm lab}$ for the ^1S line as a function of H^--ion energy for a few observation angles.

The laboratory separation in energy between the H^- lines could be expanded or contracted kinematically depending on observation angle and collision energy. The equation relating the unshifted separation to the observed separation in the laboratory frame is given by

$$E_2 - E_1 = E_{\rm lab_2} - E_{\rm lab_1} - 2[(m/M)E_{\rm H^-}]^{1/2}\cos\theta_{\rm lab} \times\cos\beta[(E_{\rm lab_2})^{1/2} - (E_{\rm lab_1})^{1/2}]. \quad (7)$$

The natural width of the line is broadened due to reaction kinematics and instrumental factors. The line profile of the electron intensity N can be determined from

$$\frac{dN}{dE_{\rm lab}} = \frac{dN}{d\phi}\frac{d\phi}{dE_{\rm lab}}, \quad (8)$$

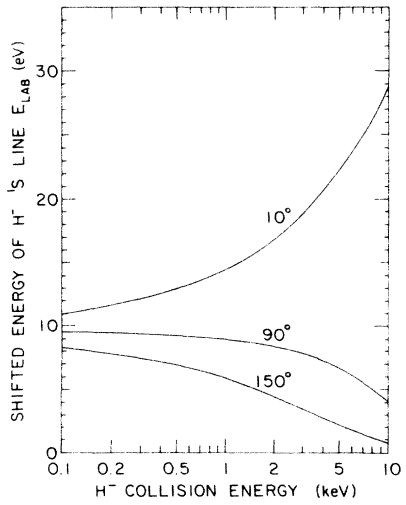

FIG. 6. Laboratory energy of 9.6-eV $(2s^2)\,^1S$ line of H^- versus H^- collision energy. The cone angle β was set equal to zero.

where $dN/d\phi$ is assumed constant owing to the axial symmetry of the ion beam. The effect on the line profile due to each instrumental and physical factor must be folded in to obtain the experimentally measured shape.

These factors are the natural lifetime of the state, the scattering angle β, the angular divergence (collimation) of the ion beam, the analyzer resolution, the energy distribution of the ion beam, the acceptance angle of the analyzer, the ion-beam collimation, and stray ac voltages on the analyzer deflection plates. Since the observed shape of the line profile of the autodetaching electrons from H^- was symmetric and closely resembled a Gaussian, it is believed that the center of the peak corresponds to the energy of the excited state. Also, since a large number of factors affected the line profile, the kinematic line broadening was analyzed by considering the effects of only the FWHM of each instrumental distribution on the observed line rather than folding all distributions in together to find the expected line profile.

The FWHM of each instrumental distribution was transformed into the laboratory frame by an expression such as

$$\Delta(E_{\rm lab})_{\rm FWHM} = \frac{\partial E_{\rm lab}}{\partial E_{\rm H^-}}\Delta(E_{\rm H^-})_{\rm FWHM}, \quad (9)$$

where in this example $\Delta(E_{\rm H^-})_{\rm FWHM}$ is the FWHM of the energy distribution of the ion beam and $\Delta(E_{\rm lab})_{\rm FWHM}$ is the FWHM of the resulting spread in the electron line profile. The partial derivatives are

$$\frac{\partial E_{\rm lab}}{\partial E} = \left[1 - \left(\frac{mE_{\rm lab}}{ME_{\rm H^-}}\right)^{1/2}\cos\theta_{\rm lab}\cos\beta\right]^{-1},$$

$$\frac{\partial E_{\rm lab}}{\partial E_{\rm H^-}} = -\left[\frac{m}{M} - \left(\frac{mE_{\rm lab}}{ME_{\rm H^-}}\right)^{1/2}\cos\theta_{\rm lab}\cos\beta\right]\frac{\partial E_{\rm lab}}{\partial E}, \quad (10)$$

$$\frac{\partial E_{\rm lab}}{\partial\theta_{\rm lab}} = -2\left(\frac{m}{M}(E_{\rm H^-}E_{\rm lab})^{1/2}\sin\theta_{\rm lab}\cos\beta\right)\frac{\partial E_{\rm lab}}{\partial E}.$$

These factors are plotted in Fig. 7 as functions of the ion energy. It can be seen that the angular effects are strongest for high collision energies and for observation angles around 45°, and that the spread in ion-beam energies is most important at low collision energies.

Two additional effects which in some collision processes can broaden lines in electron spectra are the thermal motion and the electric field of the target atom. Both of these effects can be neglected

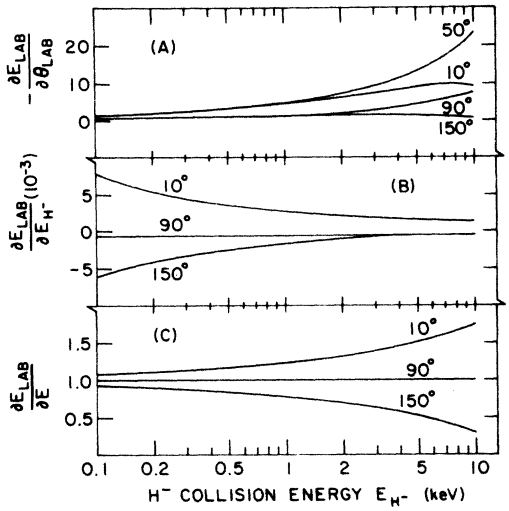

FIG. 7. Kinematic broadening factors (partial derivatives) versus H^- collision energy. (a) Angular spreads: ion scattering, beam divergence, analyzer acceptance angle. (b) Ion-beam energy distribution. (c) Natural width of line. Cone angle $\beta = 0°$.

in our case. The thermal motion of the target atom (0.02 eV) only appears as an insignificant broadening of the relative collision energy (0.1 to 10 keV). Also, because, in our case, the target is a neutral atom, its influence on the ejected electron is only that of an induced dipole and this effect is negligible.

C. Data reduction

In order to determine the unshifted electron energy E, the three quantities θ_{lab}, E_{H^-}, and E_{lab} in Eq. (4) had to be measured independently.

1. Angular setting (θ_{lab}). The analyzer was placed outside the gas cell and on top of a platform which could rotate from 9° to 80° with respect to the ion-beam axis. A stop was placed at $9.0° \pm 0.5°$. A counter, geared to the handle of the rotary feedthrough located outside the vacuum chamber, was calibrated to read directly in units of 0.1° with a negligible systematic error (less than 0.03%). The platform could be reset no better than 0.1° because of backlash and imperfections in machining.

2. Ion-beam energy distribution (E_{H^-}). Since the H^- ions were created and extracted in an electric field inside the duoplasmatron, a spread in ion energies resulted. The total potential drop across the plasma was 68 V for an arc of 1 A and a pressure of $\frac{1}{2}$ Torr. Two techniques were used to measure the energy distribution of the ion beam. At high energies, 700 eV to 10 keV, the retarding potential method, having an over-all resolution of about 20 to 30 eV, was used. For energies below 1000 eV the elastic peak due to H^- scattering from He at 10° was measured using a parallel-plate energy analyzer with a resolution of 1% FWHM. Figure 8 shows typical energy distributions of a 1-keV H^--ion beam using the retarding-potential method (RPM) and the elastically scattered H^- peak at 10°. The results of many measurements can be summarized as follows: For all ion energies the center of the energy distribution was offset 15 ± 5 eV above the voltage set on the anode of the ion source and the FWHM of the distribution was 10 ± 3 eV. The momentum transfer to the He atom in the elastic scattering collision was taken into account when calculating the offset energy.

3. Energy-scale calibration (E_{lab}). The energy

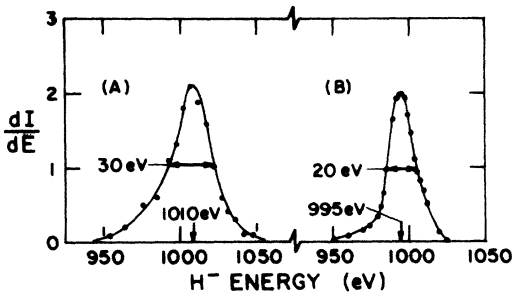

FIG. 8. Energy distribution of 1-keV H^- ion beam. (a) Retarding-potential method. (b) Elastically scattered H^- from He at 10°; energy scale has not been corrected for collision kinematics.

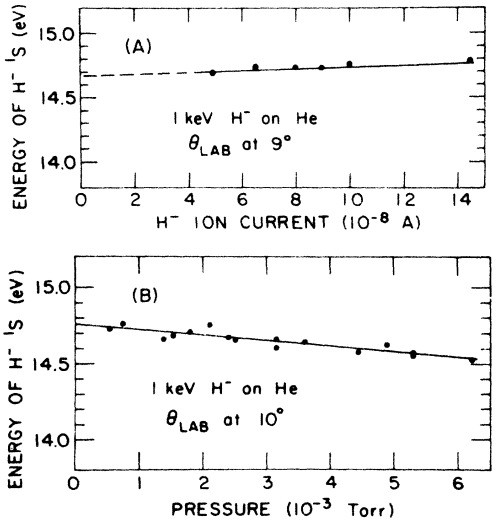

FIG. 9. Observed energy of the $(2s^2)\,^1S$ line of H^- for 1-keV H^- collisions on He observed at 9°. (a) Position of line versus ion current. (b) Position of line versus pressure of He target gas. Normally data runs were taken with a current of 1×10^{-7} A and a pressure of 5×10^{-4} Torr.

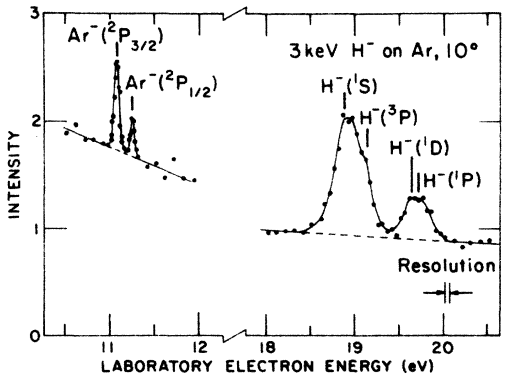

FIG. 10. Electron energy spectrum from 3-keV H^- on Ar observed at 10°. The energy scale has been corrected for contact potentials of 0.45 eV.

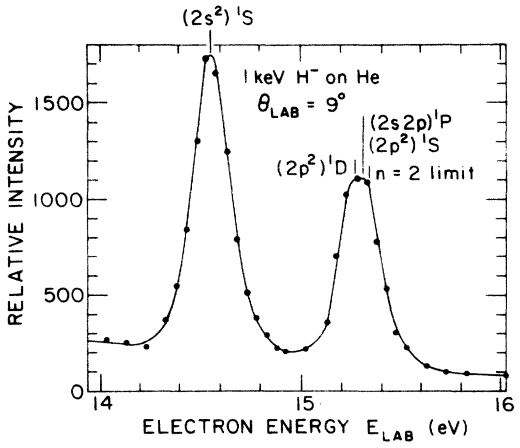

FIG. 11. Electron energy spectrum for 1-keV H^- on He observed at 9°. Indicated above the peaks are theoretical values (corrected for kinematics) assuming that the lowest energy line is the ^1S.

scale for the cylindrical analyzer was determined approximately by calculating the geometrical proportionality constant C in Eq. (1). Since small electric and magnetic fields inside the vacuum chamber altered the trajectory of the electrons, a precise calibration of the energy scale was necessary to determine E_{lab}.

By covering all surfaces first with Aquadag and then with gold black, contact-potential differences were reduced to less than 0.1 V. An additional small, electric field inside the collision region was due to the space charge of the negative H^--ion beam. Using the $(2s^2)\,^1S$ line of H^- as a source, the magnitude of this potential was determined. Figure 9 shows the change in energy of the ^1S line as a function of the ion current and the pressure of the He-gas target. The major effect of the target-gas pressure was to decrease the H^- current (due to stripping) and thus decrease the space charge. Ionization of He by H^- is a weak process.[33] In Fig. 9 it is seen that the maximum effect is less than 0.1 eV.

Another source of electric fields inside the gas cell was the biasing of the Faraday cup. Electric field plots were made for the geometry of the Faraday cup and shield used in this experiment. It was found that the electric potential at the center of the collision region was about 0.5–1.0% of the total biasing voltage. Normally +45 V ensured collection of all secondary electrons. The magnitude of this fringing field was quite dependent on the exact location of the Faraday cup inside the shield surrounding the cup. Because of this effect, all spectral measurements were made with no biasing of the Faraday cup.

The electric fields not only accelerated the electrons but also deflected them. Since the laboratory energy E_{lab} of the $(2s^2)\,^1S$ electrons was crucially

TABLE I. Positions of the H^- and the Ar^- autodetaching states (eV). Number in parentheses is uncertainty in last digit.

Investigator	Ar^- $(3p^5 4s^2)$ $^2P_{3/2}$	$^2P_{1/2}$
Kuyatt *et al*. (1965)[a]	11.08 (5)	11.25 (5)
Sanche and Schulz (1972)[b]	11.12 (3)	11.29 (3)
Average for Ar^- $^2P_{3/2}$	11.10 (4)	
Present results	11.550 (6)[c]	11.726 (6)[c]
	0.065 FWHM[d]	0.064 FWHM[d]
Kinematically shifted H^- $(2s^2)\,^1S$ for $E_{H^-} = 3005 \pm 15$ eV and $\Theta_{lab} = 10.0° \pm 0.3°$	E_{lab}	18.92(5)
Unshifted H^- $(2s^2)\,^1S$ energy	E	9.59 (3)

[a] Reference 34.
[b] Reference 35.
[c] Position not corrected for contact potential.
[d] Observed width using an analyzer resolution of 0.050 eV.

dependent on the ion energy and ejection angle [see Eq. (6) and Fig. 6], any difference between the angle of observation and the angle of electron ejection would change the expected electron energy. The measured change in the energy of the line was due, then, to a combination of the difference in electric potential and the change in the angle of observation.

Residual weak magnetic fields also affected the operation of the analyzer. The component of the magnetic field which lies *in the plane* containing the electron trajectory pushes the electron out of this plane. The slits of our analyzer were sufficiently long normal to this plane so that all electrons were transmitted. The component of a weak magnetic field *perpendicular* to the plane containing the electron trajectory affects the calibration constant C of the analyzer. An expression for the compensating change in the deflection voltage for a weak magnetic field in a parallel-plate analyzer can be derived[29] which states that

$$eV_d = C^* E, \tag{11}$$

where

$$C^* = [1 - kB/(eV_{an})^{1/2}]C.$$

B is the magnetic field perpendicular to the trajectory, V_{an} is the analyzing voltage, and k is a geometrical constant on the order of 10^{-3} $(\mathrm{eV})^{1/2}/\mathrm{mG}$. When using the constant analyzing mode for spectral measurements, Eq. (1) is modified to read for a weak magnetic field

$$eV_d = E + [(C-1)/C]eV_{an} + (k/C)(eV_{an})^{1/2}B. \tag{12}$$

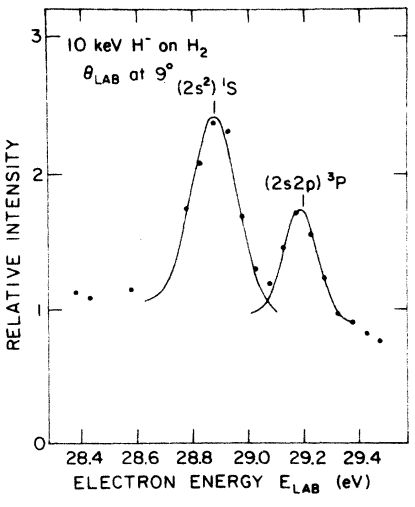

FIG. 12. Electron energy spectrum for 10-keV H^- on H_2 observed at 9°. The solid curves are Gaussian line profiles fitted to the data points after correcting for overlap between the two peaks.

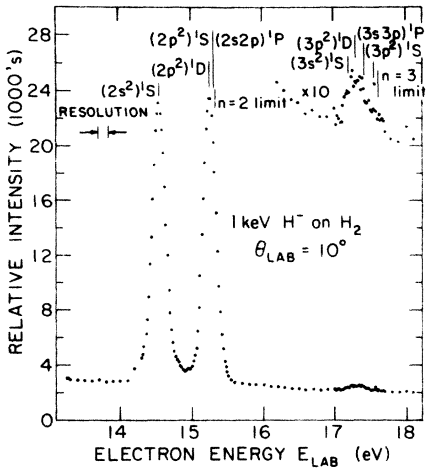

FIG. 13. Electron energy spectrum for 1-keV H^- on H_2 observed at 10°.

Note, however, that Eq. (2) still holds even for a weak magnetic field.

Since the observed laboratory energy of the electrons was shifted slightly by these external fields, a precise absolute calibration of the energy scale was performed. In collisions of H^- on Ar, two lines in the electron spectra were found at 11 eV (see Fig. 10). It was assumed that these two lines are autodetaching states of Ar^- produced in a charge-transfer collision. These same lines are found in O^- and Cl^- collisions.[3-5] No autoionizing lines of Ar were observed. The separation of the lines also agrees well with the $^2P_{3/2}$ and $^2P_{1/2}$ splitting of the Ar^+ $(3s^23p^5)$ core to which the two 4s electrons are believed bound.[34] The energy difference between the Ar^- $^2P_{3/2}$ and the H^- $(2s^2)$ ^1S lines was measured in the constant-analyzing-

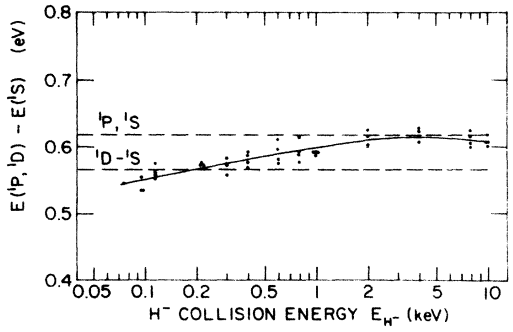

FIG. 14. Unshifted energy separation between the unresolved ^1P-^1D line and the $(2s^2)$ ^1S line versus H^- collision energy. Indicated by the dashed line are theoretical predictions for ^1D and ^1P separations. Note that below 100 eV the observed separation is less than the theoretical ^1D-^1S value. This result may indicate that the decay of the autodetaching state at low collision energies may be from a HeH^{-*} molecular state of different energy.

voltage mode at 5 eV, and using the known energy of the Ar^- resonance from the electron scattering experiments of Kuyatt, Simpson, and Mielczarek[34] and Sanche and Schulz,[35] the energy of the $H^-(2s^2)\,^1S$ level was found.

When comparing the structure in the electron energy distribution observed in electron transmission experiments with that observed in our experiment, there is an ambiguity in defining the position for the resonance energies. The Ar^- line profiles in the electron transmission experiments are asymmetric. Without theoretical calculations for the background phase shifts, it can only be assumed that the position of the resonance lies somewhere between the maximum and minimum. On the other hand, the Ar^- line shapes produced in H^- collisions are symmetric and it can be assumed that the center of the lines correspond to the resonance energy.

In Fig. 10, the peak at 19 eV is a combination of the $(2s^2)\,^1S$ and $(2s2p)\,^3P$ lines of H^-. The position in energy of the ^1S line in this spectrum was determined by unfolding the known separation of 0.17 eV between the ^3P and ^1S states; see results below. Because of the reaction kinematics, the ^3P-^1S separation increased to 0.24 eV for 3-keV collisions observed at 10°.

The separation between the H^- $(2s^2)\,^1S$ and the Ar^- $^2P_{3/2}$ lines was measured to be 7.82 ± 0.03 eV.

When an average value of 11.10 ± 0.04 eV is adopted for the energy of the Ar^- $^2P_{3/2}$ state (see Table I), the kinematically shifted value for the H^- $(2s^2)\,^1S$ line is 18.92 ± 0.05 eV for a collision of 3015 ± 5 eV observed at $10.0° \pm 0.3°$. The corresponding unshifted value is 9.59 ± 0.03 eV after correcting for recoil. Recoil accounted for a shift of 0.005 eV.

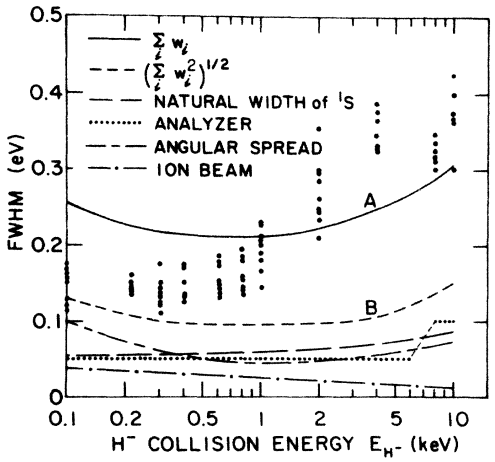

FIG. 15. FWHM versus H^- collision energy. No systematic difference was observed for the FWHM of the ^1S and the ^1P-^1D lines. Some instrumental factors affecting the broadening of the lines are indicated. Curves A and B denote the composite broadening due to all sources.

Table I lists the known positions for the Ar^- resonances along with the present results for H^- and Ar^-.

III. RESULTS

A. Energy spectra

Energy spectra of ejected electrons from incident H^- are shown in Figs. 11–13 with the energy scale corrected for contact potentials. In Fig. 11, for 1-keV H^- on He, two lines are observed. The line with lowest energy is believed to be due to the $(2s^2)\,^1S$ autodetaching state of H^-, and the other, an unresolved line which consists possibly of the $(2p^2)\,^1S$, the lowest $(2s2p)\,^1P$ and the $(2p^2)\,^1D$ levels.

TABLE II. Instrumental and physical factors which broadened the line profile.

Type	FWHM
Natural lifetime	
$(2s^2)\,^1S$	0.047 5 eV
$(2p^2)\,^1D$	0.008 8 eV
$(2s2p)\,^1P$	0.000 045 eV
$(2p^2)\,^1S$	0.002 2 eV
Deflection of H^- during collision: $\tau = \beta E_{H^-}$	2 keV-deg
Resolution of analyzer	1% of V_{an}
$V_{an} = 5$ eV (10 eV for 8- and 10-keV collisions)	
H^- energy spread	10 eV
Acceptance half-angle of analyzer	8.7×10^{-3} rad (1/2°)
Ion-beam collimation (divergence)	0.013 rad (3/4°)
ac voltage on analyzer deflection voltage (60 Hz)	0.010 eV peak to peak

The angular distribution of the second line is not isotropic and the excitation cross section differs from that of the lowest ^1S state.[23,36] Therefore, it is believed that the major contribution is due either to the ^1P or to the ^1D state and not to the ^1S.

Figure 12, observed for 10-keV H^- on H_2 at 10°, exhibits a line which we attribute to the ^3P state. Note that the reaction kinematics for 10 keV and 10° expands the energy scale, causing the ^1S and ^3P to be separated more than they would be in a reference frame at rest. The ^3P line was not observed when He was used as a target gas for collision energies up to 10 keV. If spin is conserved in these collisions, the target atom must also be excited to a triplet state if H^- is. This result gives further evidence that excitation of He is not a strong process in H^- collisions at 10 keV, consistent with observations at lower energy.[23]

The spectrum in Fig. 13 was taken for 1-keV H^- on H_2. The energy of the second lowest-lying peak for this collision is seen to agree quite well in energy with the theoretical prediction for the ^1D state, in contradistinction to the case for H^- on He. The peak at highest energy is an unresolved line below the $n=3$ level. This structure was not observed using He as a target gas.

B. Energy separation

The unshifted or true separation in energy between the H^- $(2s^2)\,^1S$ and the unresolved $(2s2p)\,^1P$ and $(2p^2)\,^1D$ line is shown in Fig. 14 as a function of ion energy for H^- on He observed at 10°. The energy separation in the laboratory frame ($E_{\text{lab}_2} - E_{\text{lab}_1}$) ranges from about 0.6 to 1.1 eV for colli-

TABLE III. Experimental values for the energies of the autodetaching states of H^- in eV. Number in parentheses is uncertainty in last digits.

State	Present experiment	McGowan and co-workers[a]	Sanche and Burrow[b]	Kleinpoppen and Raible[c]	Schulz[d]	Theory[e]
			Energy level separations			
Below $n=2$ level						
$(2s2p)\,^3P-(2s^2)\,^1S$	0.171 (10)	0.15 (3)	0.180 (10)			0.186
$(2p^2)\,^1D-(2s^2)\,^1S$						0.574
$(2s2p)\,^1P-(2s^2)\,^1S$	0.587 (10)[f]	0.57 (15)[g]	0.570 (10)[g]			0.615
$(2p^2)\,^1S-(2s^2)\,^1S$						0.615
Below $n=3$ level						
$(3s^2)\,^1S-(2s^2)\,^1S$		2.09 (3)				2.168
$(3s3p)\,^3P-(2s^2)\,^1S$		2.21 (2)				2.200
$(3p^2)\,^1D-(2s^2)\,^1S$	2.273 (22)[h]	2.33 (2)				2.254
$(3s3p)\,^1P-(2s^2)\,^1S$						2.351
$(3p^2)\,^1S-(2s^2)\,^1S$						2.472
			Absolute energy levels			
Below $n=2$ level						
$(2s^2)\,^1S$	9.59 (3)	9.56 (1)	9.558 (10)			9.545–9.585
$(2s2p)\,^3P$	9.76 (3)	9.71 (3)	9.738 (10)	9.73 (12)	9.70 (15)	9.731–9.767
$(2p^2)\,^1D$						10.119–10.156
$(2s2p)\,^1P$	10.18 (3)[f]	10.130 (15)[g]	10.128 (10)[g]			10.170–10.180
$(2p^2)\,^1S$						10.164–10.198
Below $n=3$ level						
$(3s^2)\,^1S$		11.65 (3)				11.727
$(3s3p)\,^3P$		11.77 (2)				11.759
$(3p^2)\,^1D$	11.86 (4)	11.89 (2)				11.813
$(3s3p)\,^1P$						11.910
$(3s4s)\,^1S$						12.031

[a] References 9–12, 14, 15.

[b] Reference 13.

[c] Reference 8.

[d] Reference 7.

[e] See Appendix for a listing of the more recent theoretical calculations. An average value for the theoretical results was taken in order to compare the energy difference between two states. Excluded from the average were early, less accurate calculations and Feshbach calculations in which the level shift was not computed. The average value for the $(2s^2)\,^1S$ was 9.559 eV.

[f] Line consists primarily of contributions from the $(2p^2)\,^1D$ and $(2s2p)\,^1P$ states.

[g] Line consists primarily of the $(2p^2)\,^1D$ and $(2p^2)\,^1S$ resonance.

[h] Line probably does not have any contribution from the $(3s3p)\,^3P$ state owing to spin conservation; see text and Fig. 13.

sion energies between 100 eV and 10 keV, respectively. For βE_H- equal to 2 keV deg, β could be set equal to zero with no measurable effect on the energy separations. Also indicated in the figure are the theoretical separations for the ^1D-^1S and ^1P-^1S states. The measured separation below 100 eV appears to be smaller than the predicted ^1D-^1S spacing, perhaps indicating that owing to the low ion velocity, the decay may be occuring primarily between two quasimolecular HeH^- states. The molecular potential curves may lie closer in energy than the energies of the separated $He + H^-$ atom limit.

At higher collision energies the separation is seen to increase. A possible explanation for the high-energy behavior is that the excitation cross section for the ^1P state is greater at higher energies because the excitation corresponds to a dipole transition with a transfer of only one unit of angular momentum, i.e., $H^-(1s^2)\,^1S \rightarrow H^{-*}(2s2p)\,^1P$, whereas at lower collision velocities, polarization of the H^- electron cloud can dominate with the result that higher angular momentum states can be excited.

C. Widths

The observed FWHM of both the ^1S and the unresolved ^1P-^1D lines are identical to within our experimental accuracy of ±0.05 eV. The width of the ^3P line measured at 10 keV is about 15% smaller than the ^1S. In Fig. 15 the FWHM for the ^1S and ^1P-^1D lines are shown as functions of impact energy. The natural width does not seem to change materially with collision energy. Kinematic broadening is more pronounced at higher collision energies. Note especially the relatively small width of about 0.15 eV for the 100-eV collisions. This fact implies that if the H^- decay occurs from a molecular HeH^{-*} state, the two potential curves must be nearly parallel, and also that the natural lifetimes of the quasimolecular states are no smaller than 5×10^{-15} sec. In fact, our data provide no evidence that the transition probability of H^{-*} at 100 eV differs from the transition probability of H^{-*} in a field-free region (10^{-14} sec). The excitation time for 100-eV H^- on He is much smaller than this, about 7×10^{-16} sec.[36]

Table II lists the instrumental and physical widths responsible for broadening the lines. Using Eqs. (9) and (10) the widths in Table II were transformed into the laboratory energy coordinates. Some of the larger contributions are shown in Fig. 15. A natural width of about 0.05 eV would account for about $\frac{1}{3}$ of the total width. Since the distribution of each instrumental factor is not a precisely known analytic function, it is not possible to determine the net effect of folding all the effects in together. The total widths A and B shown in Fig. 15 were found from

$$\text{A: } w_{\text{tot}} = \sum_{i=1}^{7} w_i\,, \qquad \text{B: } w_{\text{tot}} = \left(\sum_{i=1}^{7} w_i^{\,2}\right)^{1/2}. \tag{13}$$

It can be seen that at low collision energies, the widths summed as if each distribution were Gaussian (B), while at the higher collision energies Lorentzian distributions (A) seem to dominate.

D. H^- energies

Listed in Table III are the averages obtained in the present experiment for the separations between the $[(2s2p)\,^1P,\ (2p^2)\,^1D]$-$(2s^2)\,^1S$ lines for 1-keV H^- on He, between the $(2s2p)\,^3P$-$(2s^2)\,^1S$ lines for 10-keV H^- on H_2 observed at 9°, and between the $n=3$ line $(2s^2)\,^1S$ for 700-eV H^- on H_2. The energies of the states are also given, using 9.59 eV for the H^- $(2s^2)\,^1S$ state. The experimental results of McGowan and co-workers,[9-12,14,15] Sanche and Burrow,[13] Kleinpoppen and Raible,[8] and Schulz[7] are also listed along with average values from theoretical calculations; see the Appendix.

The agreement between experimental values for the ^3P-^1S separation is good. The average theoretical value lies slightly outside the experimental uncertainty of the present measurement. The separations between the $(2s^2)\,^1S$ line and the other two unresolved peaks observed in this experiment are seen to be consistent with previous electron scattering experiments and theoretical calculations.

In Table IV the measured separation between the $^2P_{3/2}$ and $^2P_{1/2}$ states of Ar^- is compared with previous experimental measurements and with the spectroscopic value for the separation between the Ar^+ $^2P_{3/2}$ and $^2P_{1/2}$ states.[37] Since the lines in the spectra from the electron transmission experiments of Kuyatt, Simpson, and Mielczarek[34] and Sanche and Schulz[35] exhibit asymmetric line profiles, and since the position of the resonance (or

TABLE IV. Energy separation between the Ar^- $^2P_{3/2}$ and $^2P_{1/2}$ levels in eV.

Present experiment	0.176 (8)
Sanche and Schulz (1972)[a]	0.172
Edwards, Risley, and Geballe (1971)[b]	0.173
Kuyatt *et al.* (1965)[c]	0.172 (3)
Spectroscopic splitting, Moore (1949)[d]	0.17755

[a] Reference 35.
[b] Observed in O^- charge-transfer collisions with Ar, Ref. 3.
[c] Reference 34.
[d] Reference 37.

TABLE V. Theoretical energy levels of H^-. All energies are in eV. The zero of the energy scale is the energy of a free electron and a hydrogen atom in the ground state. The following conversion values were used when necessary: 1 Ry (R_∞) = 13.605 83 eV, [a] 1 a.u. = $2R_\infty$. All results were corrected for the finite mass of the nucleus. $R_H = R_\infty/(1+m/M)$ = 13.598 42 eV. A number in parentheses gives the power of 10 by which the preceding number is to be multiplied.

State	E_1	Γ_1	E_2	Γ_2	Ref.
Below $n=2$ level					
$^1S^e(2s^2)$, $(2p^2)$	9.605	0.109			BS62
	9.554 [b]		10.173 [b]		O'MG65
	9.555	0.048	10.173	2.2(−3)	BT66
	9.630				H66
	9.551		10.198		HM66
	9.570 [c]	0.054 [c]			BOW67
	9.553 [d]	0.051 [d]			BOW67
	9.552 [b]		10.171 [b]		BTP67
	9.554 [b]	0.041	10.165 [b]	2.2(−3)	C67
	9.555	0.048	10.173	2.2(−3)	B68
	9.575 [b]	0.057	10.171 [b]	3.1(−3)	CR68
	9.585 [c]	0.054 [c]			BGG69
	9.582 [e]	0.050 [e]			BGG69
	9.565	0.039	10.170	3.0(−3)	CC70
	9.569	0.054	10.173	2.3(−3)	SOC71
	9.552	0.050	10.173	2.3(−3)	MO71
	9.545	0.052	10.164	4.4(−3)	CCS71
	9.552	0.047			S71
	9.552	0.047			BJ72
	9.549	0.041	10.172	2.7(−3)	CC72
	9.547	0.041			BT73
$^1P^o(2s2p)$	10.173 [b]				O'MG65
	10.258 [b]				BTP67
	10.172	4.5(−5)			B68
	10.180	2.4(−5)			SOC71
	10.170	4.5(−5)			MO71
$^3P^o(2s2p)$	9.910				H50
	9.722 [b]				O'MG65
	9.726 [b]				BTP67
	9.735	5.9(−3)			B68
	9.733	6.3(−3)			BT69
	9.767 [c]	7.6(−3) [c]			BGG69
	9.754 [e]	5.7(−3) [e]			BGG69
	9.763	8.0(−3)			SOC71
	9.735	6.8(−3)			MO71
	9.731	9.1(−3)			DD71
$^1D^e(2p^2)$	10.120	8.8(−3)			B68
	10.154 [c]	7.8(−3) [c]			OMcMc69
	10.120 [d]	8.8(−3) [d]			OMcMc69
	10.156	7.7(−3)			SOC71
	10.119	1.0(−2)			B72
Below $n=3$ level					
$^1S^e(3s^2)$, $(3p^2)$	11.727	3.9(−2)	12.031	8.6(−3)	BOW67
	11.714 [b]		12.026 [b]		O27
$^1P^o(3s3p)$	11.910	3.8(−2)			BOW67
	11.899 [b]				C72
	11.900 [b]				O72
$^3P^o(3s3p)$	11.759	4.8(−2)			BOW67
	11.741 [b]				C72
	11.742 [b]				O72
$^1D^e(3p^2)$	11.813	4.9(−2)			BOW67
	11.804 [b]				O72

TABLE V *(Continued)*

Ref.	Authors	Comment
B68	Burke (1968) (Ref. 16)	Phase shift, $1s$-$2s$-$3p$ close coupling with 20 correlation terms
B72	Bhatia (1972) [f]	Feshbach projection-operator formalism, Hylleraas type
BGG69	Burke, Gallaher, and Geltman (1969) [g]	Phase shift, close coupling with pseudostate expansion
BJ72	Bardsley and Junker (1972) [h]	Rayleigh-Ritz variational method, complex coordinates
BOW67	Burke, Ormonde, and Whitaker (1967) [i]	Phase shift, six-state close coupling
BS62	Burke and Schey (1962) [j]	Phase shift, three-state close coupling
BT66	Burke and Taylor (1966) (Ref. 42)	Phase shift, three-state close coupling with 16 correlation terms
BT69	Bhatia and Temkin (1969, 1972) (Ref. 39)	Fesnbach projection-operator formalism, 56-term Hylleraas wave function
BT73	Bhatia and Temkin (1973) (Ref. 43)	Feshbach projection-operator formalism, Hylleraas wave function
BTP67	Bhatia, Temkin, and Perkins (1967) [k]	Feshbach projection-operator formalism with 50-term Hylleraas wave function
C67	Chen (1967) [l]	Feshbach projection-operator formalism
C72	Chung (1972) (Ref. 48)	Feshbach projection-operator formalism
CC70	Chen and Chung (1970) (Ref. 44)	Feshbach projection-operator formalism
CC72	Chung and Chen (1972) (Ref. 45)	Feshbach projection-operator formalism, separation of open and closed channels
CCS71	Chen, Chung, and Sinfailam (1971) (Ref. 40)	Feshbach projection-operator formalism, coupled equations with self-consistent optical potential
CR68	Chen and Rotenberg (1968) [m]	Feshbach projection-operator formalism, simple five-parameter expansion
DD71	Drake and Dalgarno (1971) (Ref. 41)	Hylleraas–Scherr–Knight $1/z$ expansion, perturbation theory
H50	Hylleraas (1950) [n]	Five-state expansion
H66	Holøien (1966) [o]	Ritz variational method, in one-electron modified Sturmian functions
HM66	Holøien and Midtdal (1966) [p]	Ritz variational method, in one-electron modified Sturmian functions
MO71	Matese and Oberoi (1971) [q]	Phase shift, modified close-coupling formalism with several pseudostates
O72	Oberoi (1972) (Ref. 47)	Feshbach projection-operator formalism, hydrogenic and exponentially decaying wave functions
O'MG65	O'Malley and Geltman (1965) [r]	Feshbach projection-operator formalism
OMcMc69	Ormonde, McEwen, and McGowan (1969) (Ref. 12)	Phase shift, six-state hydrogenic close-coupling approximation
S71	Shimamura (1971) [s]	Phase shift, Kohn variational method, up to 70 Hylleraas terms and one nonlinear parameter

TABLE V *(Continued)*

Ref.	Authors	Comment
SOC71	Seiler, Oberoi, and Callaway (1971) [t]; see also Callaway, Oberoi, and Seiler (1970) [u]	Phase shift, algebraic close-coupling method

[a] Reference 38.
[b] Eigenvalues from Feshbach formalism, level shifts not calculated.
[c] $1s$-$2s$-$2p$ three-state hydrogenic close-coupling approximation.
[d] $1s$-$2s$-$2p$-$3s$-$3p$-$3d$ six-state hydrogenic close-coupling approximation.
[e] Pseudostate close-coupling approximation.
[f] A. K. Bhatia, Phys. Rev. A 6, 120 (1972).
[g] P. G. Burke, D. F. Gallaher, and S. Geltman, J. Phys. B 2, 1142 (1969).
[h] J. N. Bardsley and B. R. Junker, J. Phys. B 5, L178 (1972).
[i] Reference 46.
[j] P. G. Burke and H. M. Schey, Phys. Rev. 126, 147 (1962).
[k] A. K. Bhatia, A. Temkin, and J. F. Perkins, Phys. Rev. 153, 177 (1967).
[l] J. C. Y. Chen, Phys. Rev. 156, 150 (1967).
[m] J. C. Y. Chen and M. Rotenberg, Phys. Rev. 166, 7 (1968).
[n] E. Hylleraas, Astrophys. J. 111, 209 (1950).
[o] E. Holøien, Proc. Phys. Soc. Lond. A 71, 357 (1958); *ibid.* 88, 538 (1966).
[p] E. Holøien and J. Midtdal, J. Chem. Phys. 45, 2209 (1966).
[q] J. J. Matese and R. S. Oberoi, Phys. Rev. A 4, 569 (1971).
[r] T. F. O'Malley and S. Geltman, Phys. Rev. 137, A1344 (1965).
[s] I. Shimamura, J. Phys. Soc. Jap. 31, 852 (1971).
[t] G. J. Seiler, R. S. Oberoi, and J. Callaway, Phys. Rev. A 3, 2006 (1971).
[u] J. Callaway, R. S. Oberoi, and G. J. Seiler, Phys. Lett. A 31, 547 (1970).

energy of the excited state) is not necessarily the same as the position of the center of the peak, the agreement between the results derived from these two quite different collision processes is gratifying.

IV. CONCLUSION

Several lines were observed between 9 and 30 eV in the energy spectra of electrons ejected in collisions of H^- with He, Ar, and H_2. It is demonstrated that these lines are due to autodetaching states of H^-. An analysis of the reaction kinematics for the collision is given. Using lines from Ar^- for a calibration the energy of the lowest $(2s^2)\,^1S$ line is 9.59 ± 0.03 eV. The separations in energy between the $(2s^2)\,^1S$ and the $(2s2p)\,^3P$, an unresolved $(2p^2)\,^1D$ and $(2s2p)\,^1P$, and an unresolved $n=3$ line were measured. It is observed that for He the ^1P, ^1D-^1S separation is dependent on the H^- collision energy.

The present determination of the energies of these states agrees well with numerous theoretical predictions and with the experimentally observed resonances in elastic scattering of electrons on atomic hydrogen.

APPENDIX

Listed in Table V in this section are recent, significant theoretical values for the energies of the H^- states observed in the present experiment. For comparison all values were converted to eV. The energy scale was corrected for the finite mass of the nucleus. $R_H = 13.59842$ eV.[38] The effect of this correction was to reduce some of the published values by 5 to 7 meV. In some cases, where the authors corrected their calculations for the finite mass, an incorrect value for R_H was used.[18,39-41] In Table V, it is believed that all of these errors have been eliminated and the energies presented accurately.

For excited states below the $n=2$ level, the most accurate calculations were performed using a three-state hydrogenic close-coupling approximation plus 20 correlation terms by Burke and Taylor,[42] a six-state close-coupling calculation for the $(2p^2)\,^1D$ by Ormonde, McEwen, and McGowan,[12] and the Feshbach projection-operator formalism by Bhatia and Temkin[39,43] and Chen and co-workers.[40,44,45] Below the $n=3$ level, the most accurate calculations were performed using a six-state close-coupling calculation by Burke, Ormonde, and Whitaker[46] and the Feshbach formalism by Oberoi[47] and Chung.[48]

*Research supported in part by the Army Research Office, Durham, North Carolina.
†Supported in part by a NASA Traineeship.
‡Present address: Department of Physics, University of Georgia, Athens, Georgia 30602.

[1]For measurements prior to 1971 see the review by Kenneth D. Sevier, *Low Energy Electron Spectrometry* (Wiley-Interscience, New York, 1972), Chap. 6, pp. 148 and 149. More recent references are G. Gerber, R. Morgenstern, and A. Niehaus, Phys. Rev. Lett. 23, 511 (1969); J. Phys. B 5, 1396 (1972); 6, 493 (1973); F. D. Schowengerdt and M. E. Rudd, Phys. Rev. Lett. 28, 127 (1972); F. D. Schowengerdt, S. R. Smart, and M. E. Rudd, Phys. Rev. A 7, 560 (1973); M. E. Rudd, B. Fastrup, P. Dahl, and F. D. Schowengerdt, Phys. Rev. A 8, 220 (1973); N. Stolterfoht, Z. Phys. 248, 81 (1971); 248, 92 (1971); Phys. Lett. A 37, 117 (1971); N. Stolterfoht, D. Ridder, and P. Ziem, Phys. Lett. A 42, 240 (1972); L. H. Toburen, Phys. Rev. A 3, 216 (1971); A. Bordenave-Montesquieu and P. Benoit-Cattin, Phys. Lett. A 36, 243 (1971); H. W. Berry, Phys. Rev. 6, 1805 (1972); D. Burch, W. B. Ingalls, J. S. Risley, and R. Heffner, Phys. Rev. Lett. 29, 1719 (1972).
[2]Yu. F. Bydin, Zh. Eksp. Teor. Fiz. Pis'ma Red 6, 857 (1967) [JETP Lett. 6, 297 (1967)].
[3]A. K. Edwards, J. S. Risley, and R. Geballe, Phys. Rev. A 3, 583 (1971).
[4]A. K. Edwards and D. L. Cunningham, Phys. Rev. A 8, 168 (1973).
[5]D. L. Cunningham and A. K. Edwards, Phys. Rev. A 8, 2960 (1973).
[6]A. K. Edwards, J. S. Risley, and R. Geballe, in *Proceedings of the Sixth International Conference on the Physics of Electronic and Atomic Collisions* (MIT Press, Cambridge, Mass., 1969), p. 563; J. S. Risley, A. K. Edwards, and R. Geballe, in *Proceedings of the Seventh International Conference on the Physics of Electronic and Atomic Collisions* (North-Holland, Amsterdam, 1971), p. 1047; *Proceedings of the Eighth International Conference on the Physics of Electronic and Atomic Collisions* (Institute of Physics, Beograd, 1973), p. 511; and J. S. Risley and R. Geballe, *ibid.*, p. 834.
[7]G. J. Schulz, Phys. Rev. Lett. 13, 583 (1964).
[8]H. Kleinpoppen and V. Raible, Phys. Lett. 18, 24 (1965).
[9]J. Wm. McGowan, E. M. Clarke, and E. K. Curley, Phys. Rev. Lett. 15, 917 (1965); 17, 66(E) (1966).
[10]J. Wm. McGowan, Phys. Rev. Lett. 17, 1207 (1966).
[11]J. Wm. McGowan, Phys. Rev. 156, 165 (1967).
[12]S. Ormonde, J. McEwen, and J. Wm. McGowan, Phys. Rev. Lett. 22, 1165 (1969).
[13]L. Sanche and P. D. Burrow, Phys. Rev. Lett. 29, 1639 (1972).
[14]J. F. Williams and J. Wm. McGowan, Phys. Rev. Lett. 21, 719 (1968).
[15]J. Wm. McGowan, J. F. Williams, and E. K. Curley, Phys. Rev. 180, 132 (1969).
[16]P. G. Burke, Adv. At. Mol. Phys. 4, 173 (1968); see also Adv. Phys. 14, 521 (1965).
[17]K. Smith, Rep. Prog. Phys. 29, 373 (1966).
[18]J. C. Y. Chen, Nucl. Instrum. Methods 90, 237 (1970).
[19]G. J. Schulz, Rev. Mod. Phys. 45, 378 (1973); 45, 423 (1973).
[20]A. Wallis, D. L. S. McElwain, and H. O. Pritchard, J. Chem. Phys. 50, 4543 (1969).
[21]C. L. Pekeris, Phys. Rev. 126, 1470 (1962).
[22]L. M. Branscomb, Adv. Electron. Electron Phys. 9, 43 (1957); in *Atomic and Molecular Processes*, edited by D. R. Bates (Academic, New York, 1962), p. 100.
[23]J. S. Risley, Ph.D. dissertation (University of Washington, 1973) (unpublished).
[24]J. S. Risley, Rev. Sci. Instrum. 43, 95 (1972).
[25]W. Aberth and J. R. Peterson, Rev. Sci. Instrum. 38, 745 (1967).
[26]T. D. Roberts and D. S. Burch, Rev. Sci. Instrum. 35, 1067 (1964); J. Wm. McGowan, Rev. Sci. Instrum. 38, 285 (1967).
[27]T. S. Green and G. A. Proca, Rev. Sci. Instrum. 41, 1409 (1970). The third term in the Taylor-series expansion and the definition of the analyzer resolution were incorrectly stated in this paper. See Ref. 24 for the correct expressions regarding the resolution of a parallel-plate analyzer. See also W. Schmitz and W. Mehlhorn, J. Phys. E 5, 64 (1972).
[28]M. E. Rudd, Rev. Sci. Instrum. 37, 971 (1966).
[29]J. S. Risley, Rev. Sci. Instrum. 42, 267 (1971).
[30]M. E. Rudd, T. Jorgensen, Jr., and D. J. Volz, Phys. Rev. Lett. 16, 929 (1966); Phys. Rev. 151, 28 (1966).
[31]Yu. S. Gordeev and G. N. Ogurtsov, Zh. Eksp. Teor. Fiz. 60, 2051 (1971) [Sov. Phys.—JETP 33, 1105 (1971)].
[32]See the 1973 article by Gerber, Morgenstern, and Niehaus, Ref. 1.
[33]Ya. M. Fogel', A. G. Koval', and Yu. Z. Levchenko, Zh. Eksp. Teor. Fiz. 38, 1053 (1960) [Sov. Phys.—JETP 11, 760 (1960)].
[34]C. E. Kuyatt, J. A. Simpson, and S. R. Mielczarek, Phys. Rev. 138, A385 (1965).
[35]L. Sanche and G. J. Schulz, Phys. Rev. A 5, 1672 (1972).
[36]J. S. Risley, A. K. Edwards, and R. Geballe, Phys. Rev. Lett. 29, 904 (1972).
[37]C. E. Moore, *Atomic Energy Levels*, Circ. Natl. Bur. Stand. No. 467 (U. S. GPO, Washington, D. C., 1949), Vol. 1.
[38]B. N. Taylor, W. H. Parker, and D. N. Langenberg, Rev. Mod. Phys. 41, 375 (1969).
[39]A. K. Bhatia and A. Temkin, Phys. Rev. 182, 15 (1969); Phys. Rev. A 6, 562(E) (1972).
[40]J. C. Y. Chen, K. T. Chung, and A. L. Sinfailam, Phys. Rev. A 4, 1517 (1971).
[41]G. W. F. Drake and A. Dalgarno, Proc. R. Soc. Lond. A 320, 549 (1971).
[42]P. G. Burke and A. J. Taylor, Proc. Phys. Soc. Lond. 88, 549 (1966); see also the tabulated values in Ref. 16.
[43]A. K. Bhatia and A. Temkin, Phys. Rev. A 8, 2184 (1973).
[44]J. C. Y. Chen and K. T. Chung, Phys. Rev. A 2, 1892 (1970).
[45]K. T. Chung and J. C. Y. Chen, Phys. Rev. A 6, 686 (1972).
[46]P. G. Burke, S. Ormonde, and W. Whitaker, Proc. Phys. Soc. Lond. 92, 319 (1967).
[47]R. S. Oberoi, J. Phys. B 5, 1120 (1972).
[48]K. T. Chung, Phys. Rev. A 6, 1809 (1972).